Surfaces and Interfaces 72 (2025) 107196

Contents lists available at ScienceDirect

Surfaces and Interfaces

journal homepage: www.sciencedirect.com/journal/surfaces-and-interfaces

Study on synergistic antifouling of super slippery drug-loaded modified film based on electrospinning-electrospray in situ process

Fengqin Li, Yang Zhou, Yuxue Hu, Xiaoming Feng *, Guizhong Tian *

College of Mechanical Engineering, Jiangsu University of Science and Technology, Zhenjiang, 212100, PR China

ARTICLE INFO

Keywords:
Porous matrix
Modified composite film
Electrospinning-electrospray in situ process
Synergistic antifouling

ABSTRACT

Marine biofouling is a significant threat to the economic efficiency and sustainable development of global marine industries. Conventional antifouling coatings, which rely on a single antifouling mechanism, struggle to adapt to complex marine environments. The challenge of seamlessly integrating multi-level antifouling strategies into coatings through a facile approach remains unresolved. This study innovatively developed a super slippery drug-loaded nanofiber composite coating with dynamic interfacial regulation capabilities through an integrated electrospinning-electrospray in situ process. A biodegradable polymer, poly(ε-caprolactone) (PCL), served as the electrospinning base material, into which the eco-friendly antifoulant DCOIT (4,5-dichloro-2-n-octyl-4-isothiazolin-3-one) was incorporated during fiber formation, constructing a porous drug-loaded nanofiber matrix. Concurrently, in situ electrospray was employed to dynamically deposit silica (SiO_2) nanoparticles onto the nanofiber surfaces, forming a modified porous matrix. Subsequent infusion of lubricant oil produced a super slippery drug-loaded modified film (SSLID). The modified film demonstrated excellent hydrophobicity and antifouling performance, achieving synergistic multi-level antifouling effects. This fabrication strategy provides an efficient and adaptable approach for developing functional composite coating films, offering broad application prospects in marine antifouling technologies.

1. Introduction

Marine biofouling represents a significant threat to the economic viability and sustainable development of global marine industries. The development of cost-effective and eco-friendly antifouling coatings with long-term durability is widely regarded as a critical direction for advancing marine antifouling technologies [1–5]. However, traditional coatings based on single antifouling strategies encounter limitations, such as performance degradation over time, frequent maintenance requirements [6,7], and inadequate adaptability to complex marine environments due to their lack of broad-spectrum antifouling capabilities [8]. In contrast, integrating multiple strategies—including bioinspired low adhesion, dynamic surface renewal, and controlled release of eco-friendly antifoulants—provides a more efficient design paradigm. These synergistic mechanisms endow coatings with multifunctional properties, such as antibacterial activity, anti-adhesion, and pollutant degradation, thereby improving antifouling efficacy, prolonging service life, and minimizing failure risks [9–11].

Electrospinning technology has become a preferred method for fabricating functional substrate films attributed to its unique porous structure and adaptability in various fields [12–17]. For instance, in biomedical applications, Lan et al. [18] reviewed the preparation techniques and controlled release behavior of multi-drug micro/nano multifunctional films under electrospinning process. Xing et al. [19] focused on medical applications and systematically summarized the implementation of electrospinning technology for preparing multi-material functional membranes. Conventional electrospinning enables the production of continuous fibers with diameters ranging from tens of nanometers to micrometers. However, achieving functionalization often necessitates additional post-processing steps, thereby increasing both complexity and costs [20]. Powell et al. [21] employed plasma treatment as a post-fabrication modification to achieve desired wettability, while Xu et al. [22] utilized the electrospray-electrospinning layer-by-layer deposition process to prepare multi-layered membranes, which introduced operational challenges and impeded cost-effective large-scale production. Furthermore, encapsulating modification particles entirely within fibers may compromise surface wettability regulation. Notably, electrospinning and electrospray are twin technologies

* Corresponding authors.
E-mail addresses: xmfeng@just.edu.cn (X. Feng), justtgz@163.com (G. Tian).

https://doi.org/10.1016/j.surfin.2025.107196
Received 28 May 2025; Received in revised form 3 July 2025; Accepted 12 July 2025
Available online 13 July 2025

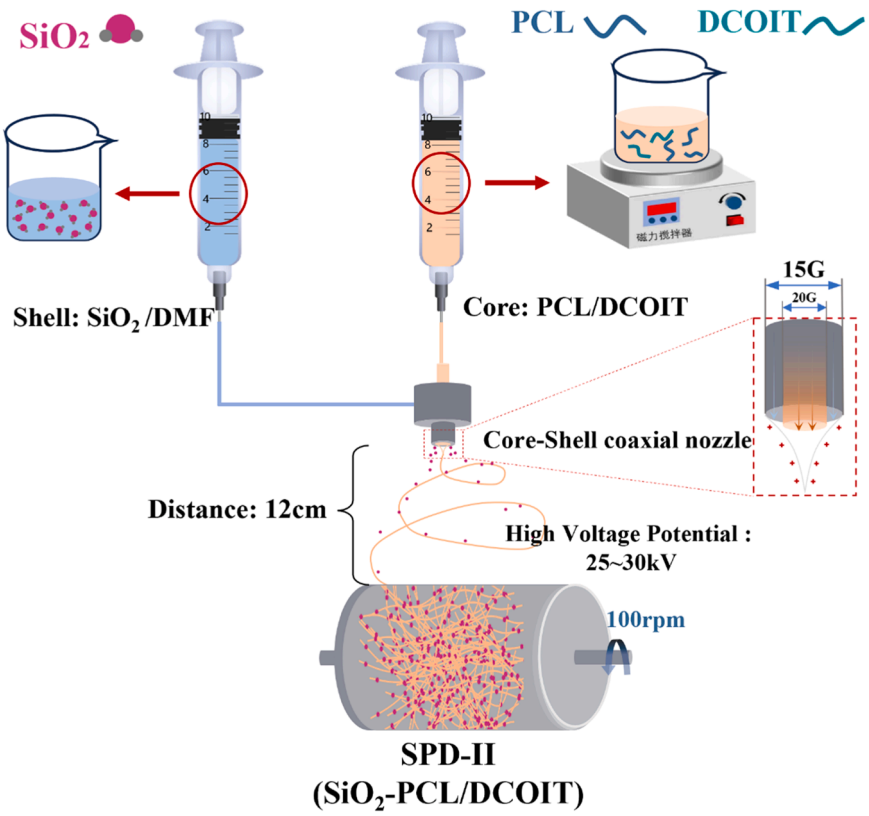

Fig. 1. Schematic diagram of the electrospinning-electrospray in situ process for preparing SiO_2-PCL/DCOIT nanofiber film.

based on identical electrohydrodynamic (EHD) principles [23,24]. Strategic integration of these two methods could synergize their respective advantages, offering a mutually beneficial solution for advanced functional coatings.

Recent studies have explored the integration of multifunctional properties into electrospun nanofiber films. In engineering applications, Si et al. [25] developed a superhydrophobic composite protective film using a one-step electrospinning-electrospray hybrid process, demonstrating potential applications in safeguarding personnel operating in extreme environments. Separately, Wang et al. [26] engineered core-shell fibers with hyper-encapsulated architectures via coaxial electrospinning, achieving simultaneous hydrophobicity and flame-retardant performance. In current marine antifouling research, Gao et al. [27] investigated polyurea-based functional coatings embedded with TiO_2 particles for enhanced antifouling and drag-reduction capabilities. Pourhashem et al. [28] comprehensively reviewed the role of various nanomaterials in developing polymeric antifouling coatings and analyzed performance enhancement strategies through hybridization of nanomaterials with tailored chemical agents. In addition to utilizing inorganic particles for antibacterial purposes, antifouling research based on individual mechanisms (e.g., biomimetic micro/nano surfaces, hydrophilic/hydrophobic properties, low adhesion, and eco-friendly controlled drug release) is being conducted [8,29]. However, only a limited number of researchers have successfully achieved the effective coupling of multiple antifouling mechanisms. If multiple antifouling mechanisms be integrated into composite coatings via the straightforward and versatile electrospinning technique, this approach would represent a novel paradigm for the design and development of marine antifouling coatings.

In this study, a novel composite SSLID (Super SLIppery Drug-loading modified film) was developed to achieve long-term and stable antifouling performance through the synergistic integration of super low adhesion properties, dynamic surface antifouling (DSA), and eco-friendly antifouling agents. Specifically, an in situ electrospinning-electrospray hybrid process with coaxial nozzles (replacing single-nozzle configurations) was employed to dynamically deposit silica nanoparticles (SiO_2 NPs) onto the exterior of biodegradable poly (ε-caprolactone) (PCL) nanofibers, thereby achieving hydrophobic surface modification. Simultaneously, PCL served dual functions as both a carrier for the eco-friendly antifoulant DCOIT and an electrospinning matrix. The fiber entanglement during spinning resulted in a modified porous substrate (SiO_2-PCL/DCOIT). Subsequent infusion of lubricant oil stabilized the composite nanofiber film (SSLID). The resulting film demonstrates exceptional hydrophobicity, low adhesion, and multi-mechanism antifouling capabilities, while enabling dynamic surface self-renewal. The synergistic strategy proposed here can be generalized to diverse biodegradable polymer systems, providing critical insights for advancing antifouling coatings in marine applications such as ship transportation, deep-sea equipment, port infrastructure, and subsea pipelines.

2. Materials and methods

2.1. Materials

Poly(ε-caprolactone) (PCL, Mw=80,000 g/mol), N,N-dimethylformamide (DMF, AR grade, 99.5 %), dichloromethane (DCM, ≥99.5 %), DCOIT (4,5-dichloro-2-n-octyl-4-isothiazolin-3-one), silica nanoparticles (SiO_2, purity 99.8 %, particle size: 7-40 nm), and dimethylsilicone oil (viscosity:100 mPa·s) were procured from Shanghai Aladdin Biochemical Technology Co., Ltd. All materials were utilized as received without further purification. Gram-negative *Escherichia coli* (*E. coli*, strain CMCC 44,102) and Gram-positive *Bacillus* sp. (strain ATCC 6633) were acquired from the Shanghai Microbiological Culture Collection Co., Ltd. The electrospinning setup, including polytetrafluoroethylene (PTFE) tubing, a syringe pump (microfluidic control), stainless steel needles, coaxial nozzles, aluminum foil collectors, and a high-voltage power supply, was sourced from Beijing Ucalery

Table 1
Preparation methods and material compositions for various drug-loaded porous fiber films.

Sample name	Methods of Preparation	Ratio of PCL Solute(wt %)	SiO_2 NP (mg/mL)	Silicone Oil	Instructions for preparation
13 %PCL/DCOIT	Electrospinning	13 %	/	/	Optimization of porous drug-loaded fibrous matrix
15 %PCL/DCOIT		15 %	/	/	
17 %PCL/DCOIT		17 %	/	/	
19 %PCL/DCOIT		19 %	/	/	
SPD-I	Electrospinning	15 %	50	/	Hydrophobic and lipophilic modified fiber matrix
SPD-II	Electrospinning- spraying	15 %	50	/	
SSLID	Electrospinning-spray & Injection	15 %	50	50 μL	Super slippery drug-loaded modified matrix film

Technology and Development Co., Ltd.

2.2. Preparation of PCL/DCOIT drug-loaded porous nanofiber film

A mixture of DCM/DMF (1.35:1, v/v) was prepared to formulate PCL polymer solutions with concentrations of 13 %, 15 %, 17 %, and 19 % (w/v). Subsequently, 0.2 g DCOIT drug was added to each solution, followed by magnetic stirring at room temperature for 2 h to ensure homogeneity. The Electrospinning process parameters were set as follows: flow rate of 2mL/h, working distance of 12 cm, voltage of 18 kV. Nanofibers were collected on a high-speed rotating shaft collector covered with aluminum foil for about 20 min. After electrospinning, the fibrous film was transferred to a vacuum oven at 30 °C for 24 h to completely remove any residual solvent. The resulting PCL/DCOIT drug-loaded porous nanofiber film had a thickness of approximately 40 μm.

2.3. Preparation of hydrophobic modified nanofiber film

2.3.1. Preparation of SiO_2/PCL/DCOIT nanofiber film based on electrospinning one-step method

A total of 0.5 g of SiO_2 nanoparticles were dispersed into a 15 % (w/v) PCL/DCOIT drug-loaded polymer solution. The resulting mixture was subjected to ultrasonic treatment for 30 min using an ultrasonic oscillator (Jiemeng JP-020, 40 kHz) to ensure the formation of a completely homogeneous inorganic-organic blend solution. Subsequently, the prepared solution was transferred into a 10 mL syringe. The SiO_2/PCL/DCOIT fiber film (referred to *As spd*-I) was successfully fabricated according to the optimized spinning parameters for the drug-loaded polymer, with its thickness precisely controlled at 40 ± 2 μm.

2.3.2. Preparation of SiO_2-PCL/DCOIT hybrid nanofiber films based on electrospinning-electrospray in situ process

To further enhance the modification performance of the porous nanofiber films, SiO_2-PCL/DCOIT hybrid fiber films (referred to *A. spd*-II) were prepared by the electrospinning-electrospray in situ process. The schematic diagram of the specific preparation procedure is presented in Fig. 1.

Fig. 1 illustrates the preparation process and the equipment utilized in the electrospinning-electrospray in situ modification process. The setup includes two precision syringe pumps, a high voltage power supply, a collector, and a coaxial nozzle. The coaxial nozzle consists of two stainless steel needles: the inner needle has an outer diameter of 0.61 mm (20 G specification), while the outer needle has an inner diameter of 1.36 mm (15 G specification). To improve the binding efficiency of nanoparticles to the fiber surface, the polymer solution and the inorganic modification solution were separately loaded into two syringes and connected onto custom-designed coaxial core sheath needles (20 G for the inner channel and 15 G for the outer channel). Specifically, the inner channel was linked to a 15 % PCL/DCOIT polymer solution for electrospinning, whereas the outer channel was attached to a SiO_2/DMF suspension for electrospray. The spinning parameters were set as follows: an internal fluid flow rate 2.5 mL/h, an external fluid flow rate 0.2 mL/h, an applied voltage of 25-30 kV, a collection distance between nozzle and rotating drum of 12 cm, and a roller speed of 100 rpm. The thickness of the resulting SiO_2-PCL/DCOIT hybrid fiber film (SPD-II) was precisely controlled at 40 ± 2 μm. All nanoporous fibers were prepared under ambient conditions of 25 °C and 35 % relative humidity.

2.4. Preparation of oil-loaded and drug-loaded super slippery modified film

Fifty microliters (50 μL) of silicone oil were injected into the SPD-II matrix film prepared above. To ensure complete penetration and uniform distribution of silicone oil within the porous structure, the oil-filled samples were subjected to a vacuum treatment in a vacuum drying oven for 2 h, resulting in the formation of super slippery drug-loaded films (referred to as SSLID). The material compositions and preparation methods for each sample are summarized in Table 1.

2.5. Characterizations

2.5.1. Solution characterization

The apparent viscosity of each polymer solution at different shear rates was measured using a rotary rheometer (MCR92, Anton Paar, Austria) within the range of 0.1 to 20 s^{-1} at 25 °C. Based on the power-law model, the relationship between shear stress(τ) and shear rate can be fitted using Eq. (1), and the apparent viscosity(η) at different shear rates can be calculated using Eq. (2) [30]:

$$\tau = k_1 \gamma^n \tag{1}$$

$$\eta = k_2 \gamma^{m-1} \tag{2}$$

Where τ(Pa), γ(s^{-1}), and η respectively represent the shear stress, the shear rate, and the apparent viscosity; k_1/k_2 (Pa·s^n) denotes the consistency coefficient; n denotes the flow characteristic index; and m indicates the non-Newtonian exponent of the material. For pseudoplastic fluids, $m\langle 1$; for rheopectic fluids, $m\rangle 1$; whereas, for Newtonian fluids, $m = 1$.

2.5.2. Characterization of nanofiber films

The morphology of several nanofiber samples was characterized using scanning electron microscope (SU8600, Hitachi, Japan), and the chemical element composition of nanofibers was quantitatively analyzed via energy dispersive spectroscopy (EDS, EDAX APEX). Prior to these measurements, the samples were coated with gold under vacuum conditions to ensure excellent electrical conductivity. The average diameter of the nanofiber filaments in the SEM images ($n > 50$) was analyzed using ImageJ software. Macro and micro morphological images of lubricating oil molecules within the fiber matrix were captured using a high-resolution digital video microscope (HRX-01, Hirox, Japan).

2.6. Hydrophobic and self-cleaning properties of porous nanofiber films

The hydrophobic properties of PCL/DCOIT nanofiber films with different concentrations and the SPD-II modified nanofiber films (SiO_2-PCL/DCOIT) were evaluated using a contact angle measurement

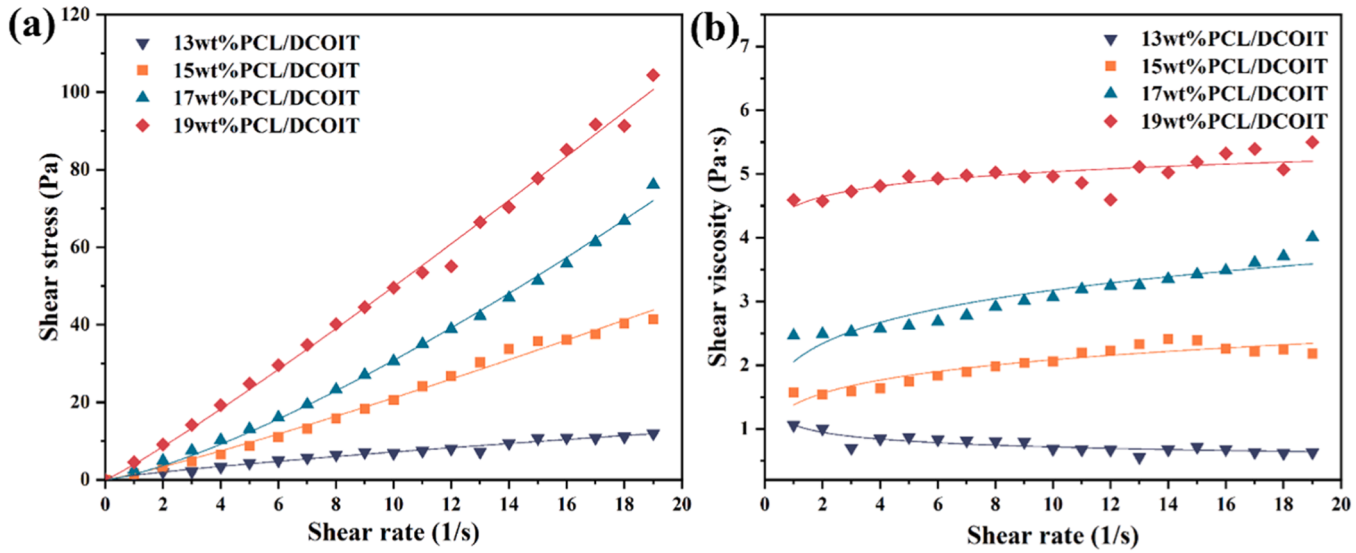

Fig. 2. Viscosity characteristics analysis of drug-loaded polymer solution at different concentrations: (a) shear stress, (b) shear viscosity.

instrument (Theta Lite, BIOLIN Shanghai, China). The droplet volume was set to 5 μL. To ensure data reliability, five replicate measurements were conducted for each sample, and the results were averaged. To test the self-cleaning performance of the SPD-II samples, they were mounted on an 8° inclined glass plate. Upon water droplet impact, surface contaminants were adsorbed and removed, and the SPD-II was immersed in methylene blue-stained water to verify its anti-fouling ability.

2.7. Mechanical stability of modified fibrous films

The mechanical stability of the surface micro-nano structure of SPD-II nanofiber films was assessed through sandpaper abrasion tests and tape peeling tests. For the sandpaper abrasion test, the film was cut into appropriately sized dimensions and placed face-down on 1500-grit sandpaper. A load of 2 N was applied while dragging the sample horizontally forward by 100 mm, followed by backward dragging over the same displacement, constituting one abrasion cycle. In the tape peeling experiment, the sample was mounted on a glass slide. Adhesive tape was pressed onto the film surface and then peeled off slowly until complete separation was achieved, completing one peeling cycle. Finally, the water contact angles after abrasion and peeling treatments were determined separately. Five replicate measurements were conducted for each sample, and the average value was reported as the final result.

2.8. Dynamic roll-off behavior and anti-adhesion stability of modified films

The sliding angles of SPD-II and SSLID samples were accurately measured using a PCO Dimax S1 high-speed camera to evaluate their sliding performance. Simultaneously, water droplets and component droplets were deposited onto the surface of the super-slippery SSLID to observe the dynamic process of different liquid droplets sliding off the surface. To further evaluate the roll-off stability of the SSLID composite film, a knife scratch test was conducted. The SSLID surface was scratched with a sharp tool to simulate mechanical damage under practical conditions. Subsequently, the sliding behavior of water droplets on the inclined 10° surface of the scratched SSLID composite film was observed.

2.9. Antifouling performance test

Considering the significant differences in size and morphology between Gram-positive and negative bacteria, these two types of bacteria were selected to investigate the antibiological fouling properties of the film [31]. The antifouling performance of the samples was evaluated by examining the bactericidal efficacy and adhesion behavior of representative Gram-positive and negative marine bacteria.

2.9.1. Antifouling adhesion test

The number of bacteria adhered to the sample surface was quantitatively analyzed using the plate method, with the colony count on the agar plate serving as an indicator of the antifouling performance of the SSLID composite film at different time points. Gram-negative *E. coli* was selected as a representative strain for antifouling testing, and the dynamic antifouling effect of the film was evaluated by simulating the fluid environment using an oscillating box [32]. Initially, *E. coli* colonies grown on agar medium were harvested using an inoculating loop and transferred to LB liquid medium for incubation at 37 °C for 24 h under shaking conditions at 120 rpm. Subsequently, SSLID samples were immersed in 20 mL of *E. coli* suspension (turbidity: 0.9) at 37 °C for soaking periods of 1, 10, 20, and 30 days under shaking conditions at 100 rpm. To maintain bacterial viability, fresh bacterial suspension and medium were replaced every 5 days. At each sampling time point, the samples were gently washed twice with PBS buffer to remove loosely adherent bacterial cells. The samples were then sonicated in PBS buffer for 20 min. Next, 5 μL of the sonicated solution was spread onto agar plates and incubated overnight at 37 °C. After incubation, the number of colonies on the agar plates was observed and counted, and the coverage of *E. coli* on the coated surface was analyzed using ImageJ software. The anti-adhesion tests for Gram-positive *Bacillus* were also conducted following the same procedure.

2.9.2. Antibacterial test

Agar diffusion method was employed to evaluate the antibacterial efficacy of nanofiber films (SPD-I, SPD-II) and oil-injected SSLID under both full-oil and oil-run-out conditions against *E. coli* and *Bacillus*, respectively. PCL, SiO_2-PCL fibrous films (SP-II), and SSLI, which were drug-free, served as the control group. The films were cut into circular disks with a diameter of approximately 6 mm and used as experimental samples. Initially, Gram-negative *E. coli* colonies were inoculated into LB medium and incubated overnight at 37 °C. Subsequently, the optical density (OD) at 600 nm was measured using a spectrophotometer, and the bacterial concentration was adjusted to a turbidity of 0.9. Next, 100 μL of the *E. coli* suspension was evenly spread onto LB agar plates using sterile cotton swabs and coating rods. The samples of each group were then placed on the agar plates and incubated at 37 °C for 24 h. The

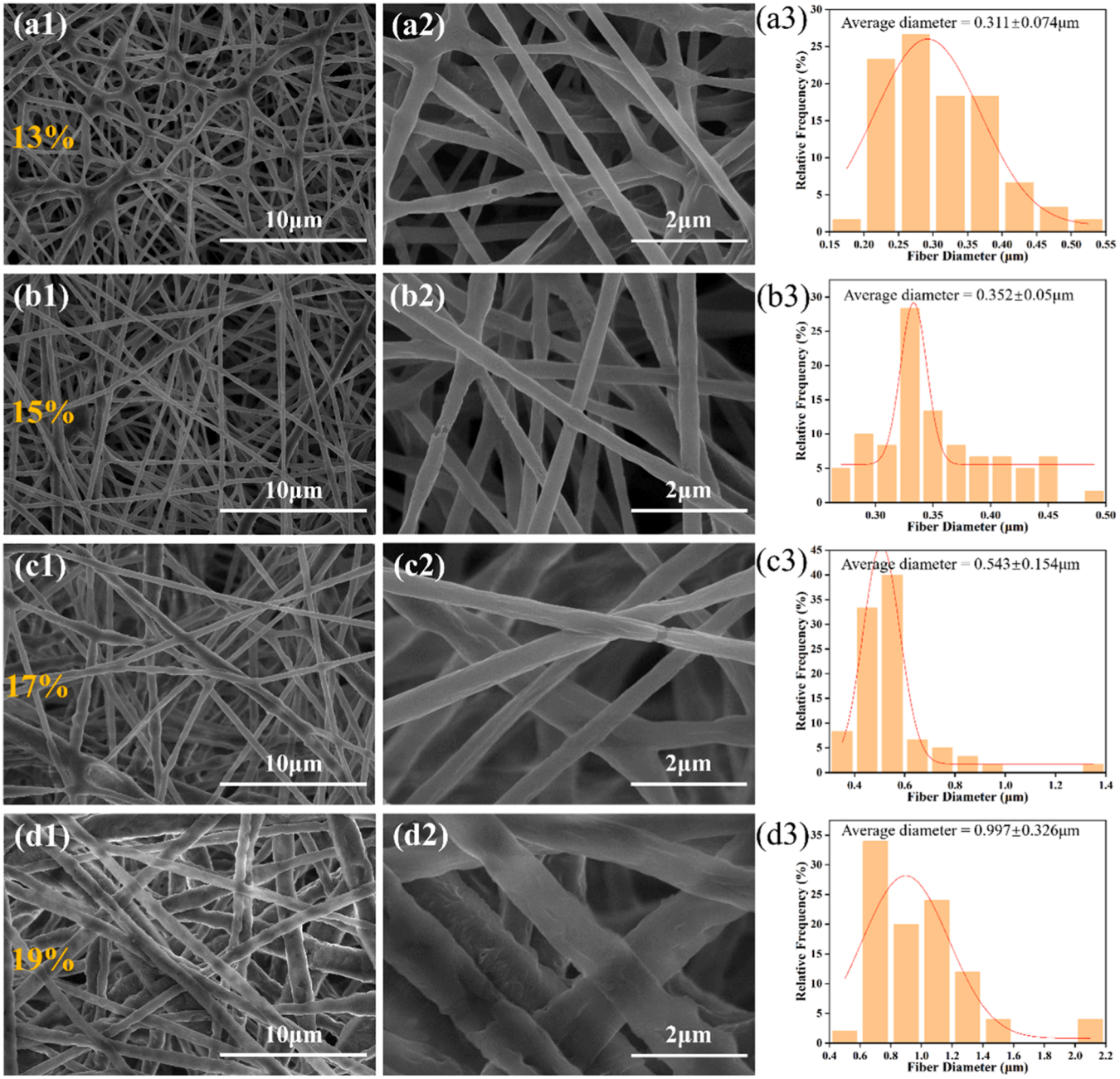

Fig. 3. SEM images, high-magnification images, and fiber diameter histograms of PCL/DCOIT nanofiber films with four polymer concentrations (13 %, 15 %, 17 %, and 19 %).

diameters of the inhibition zones were measured using ImageJ software. Similarly, the antibacterial test for Gram-positive *Bacillus* was also conducted following the experimental procedure described above.

3. Results and discussion

3.1. Polymer solution analysis

At low viscosity, it is challenging for spinning solutions to form continuous fibers, whereas high viscosity prevents jet ejection [33]. The appropriate viscosity can produce high-quality continuous fibers. Therefore, in order to optimize the spinning conditions, the rheological characteristics of the spinning solution at room temperature (25 °C) were first analyzed, and the results are shown in Fig. 2.

Fig. 2a shows the relationship between shear rate and shear stress for four PCL/DCOIT solution concentrations (13 %, 15 %, 17 %, and 19 %). It is evident that the shear stress does not exhibit a proportional relationship with the shear rate. Given that the shear stress increases with the shear rate, it can be inferred that these solutions behave as non-Newtonian fluids. At the same shear rate, the shear stress increases with the increasing content of PCL. As the concentration of PCL rises from 13 %(w/v) to 19 %, the power-law consistency index (k_1) of the spinning solution increases from 1.148 to 3.999, indicating that the shear stress at a unit shear rate becomes larger. When the PCL concentration is 13 %, the fluid exhibits pseudoplastic behavior (shear-thinning fluid, $n = 0.794$). As the PCL concentration increases from 15 % to 19 %, the fluid transitions to dilatant behavior (shear-thickening fluid). The flow characteristic index (n) initially increases from 1.137 to 1.322 and subsequently decreases to 1.095, suggesting that the viscosity of the 17 % PCL/DCOIT solution changes most significantly with variations in the

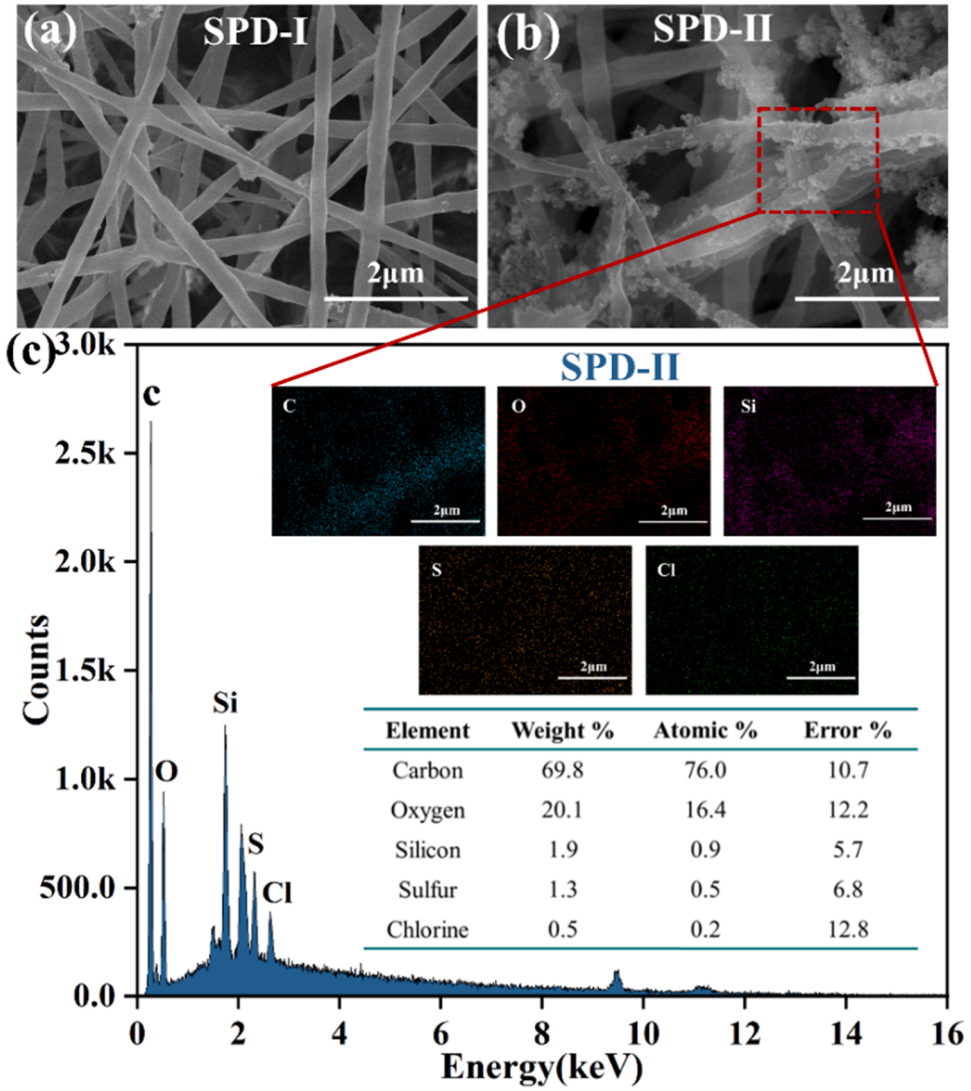

Fig. 4. SEM images and energy spectrum analysis of SiO_2-modified fiber films: (*A) spd*-I prepared by one-step electrospinning; (b) SPD-II prepared by electrospinning-electrospray in situ process; (c) EDS spectra and elemental composition analysis of SPD-II.

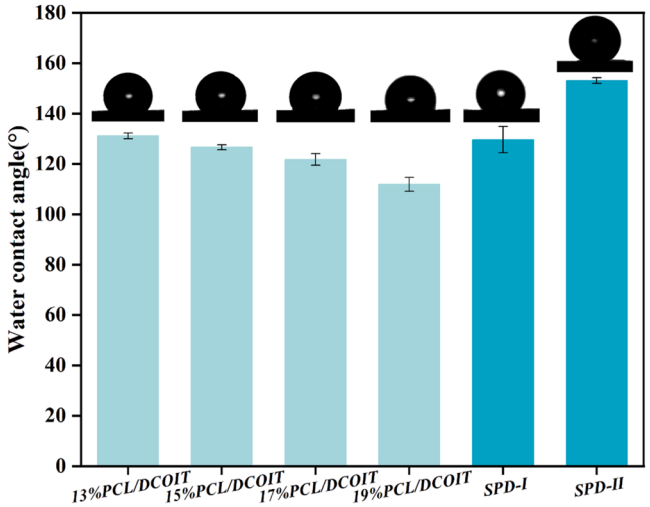

Fig. 5. Water contact angles of drug-loaded nanofiber films with varying polymer concentrations (13 %, 15 %, 17 %, 19 %) and modified SPD-I and SPD-II composite films.

shear rate. Therefore, considering the influence of the consistency coefficient and flow characteristic index, the 15 % PCL/DCOIT solution, which exhibits the relatively lower consistency coefficient and flow index close to 1, was selected as the optima spinning solution.

Fig. 2b illustrates the shear viscosity of the solution across a range of shear rates from 20 s^{-1}. Given that the viscosity of the spinning solution as it passes through the spinneret is critical to the elongation and other properties of the nanofibers, the shear rate γ at the spinneret outlet can be approximately estimated using Eq. (3) [34]

$$\gamma = \frac{4Q}{n\pi R^3} \tag{3}$$

Where Q represents the volumetric flow rate of spinning solution (mm^3/s), n and R denote the number of holes and radius of the spinning nozzle (mm), respectively.

At a low shear rate (γ=1.0 s^{-1}), the shear viscosities of the four concentration solutions were 1.06 Pa·s, 1.569 Pa·s, 2.464 Pa·s, and 4.592 Pa·s, respectively, which were consistent with the power-law fitting obtained from Eq. (2). Through fitting analysis, the corresponding fluid consistency coefficients (k_2) were determined to be 1.066, 1.373, 2.051, and 4.482, while the power-law indices (m) were calculated as 0.826, 1.181, 1.19, and 1.05, respectively. This phenomenon

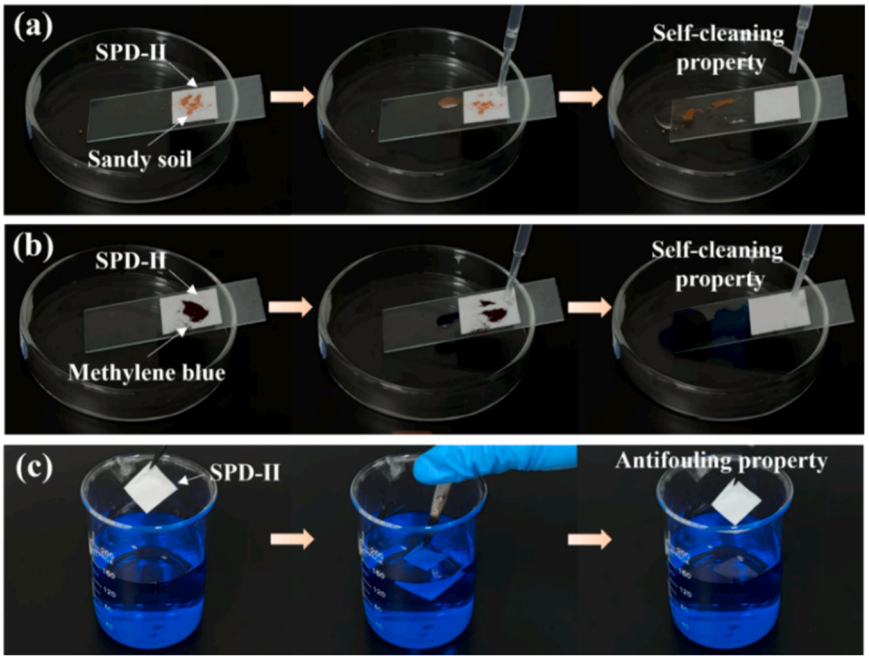

Fig. 6. Self-cleaning test of SPD-II nanofiber film: (a) sandy soil, (b) methylene blue, and (c) stained water.

can primarily be attributed to the formation of more compact and ordered structures by particles or polymer chains within the fluid under high shear rates, thereby increasing internal friction and flow resistance. To minimize the shear-rate dependence of apparent viscosity (i.e., to maintain relatively constant fluid viscosity under different shear conditions), the spinning solution should ideally exhibit near-Newtonian fluid behavior. Consequently, the 15 wt % PCL/DCOIT solution was selected as the optimal spinning solution, which is in agreement with the findings from stress analysis.

3.2. Structural and morphological analysis of nanofiber films

3.2.1. PCL/DCOIT nanofiber films

The mechanical strength, durability, and stability of nanofiber films are significantly influenced by factors including fiber diameter, material properties, and surface structure [35]. Therefore, to achieve optimal synergistic effects between nanofiber films and electrospray technology, it is essential to perform in-depth investigation and optimization of these key parameters to ensure their performance satisfies specific application requirements.

In this study, DCOIT was blended into the PCL matrix, which not only improved the antibacterial activity of the material, but also combined with the degradation characteristics of PCL to achieve long-term inhibition of bacterial growth and reproduction, effectively extending the anti-fouling aging. The microscopic morphology and fiber diameters of drug-loaded nanofiber films with four polymer concentrations (13 %, 15 %, 17 %, and 19 %) are shown in Fig. 3.

SEM images reveal that the incorporation of DCOIT does not significantly alter the porous architecture of PCL nanofiber films. Each individual nanofiber exhibits a bubble-free, dense morphology, with no discernible phase separation observed between the PCL matrix and DCOIT. This observation indicates homogeneous dispersion of DCOIT within the polymer matrix, which preserves the structural integrity and functional efficacy of the nanofibers. Such uniform distribution facilitates long-term stable antibacterial performance, rendering the composite films suitable for practical applications requiring sustained antimicrobial activity. Meanwhile, as shown in the enlarged plot in the second column of Fig. 3, the nanofiber diameter gradually increases with increasing PCL concentration. The fiber diameter histogram in the third column clearly illustrates the diameter distribution of these fibers, with average diameters of 0.311 ± 0.074 μm, 0.352 ± 0.050 μm, 0.543 ± 0.154 μm, and 0.997 ± 0.326 μm, respectively. This further verifies the relationship between fiber diameter and PCL concentration.

Among the four solutions, the 15 wt % PCL/DCOIT spinning solution was identified as the most ideal option in this study due to its uniform fiber diameter distribution and excellent morphological characteristics. This result is in agreement with the analysis of polymer solutions in Section 3.1. Based on these results, nanofibers with a broad range of fiber diameters and a relatively uniform distribution were chosen for the subsequent procedures.

3.2.2. SiO_2-modified PCL/DCOIT nanofiber films

To further compare the encapsulation and modification effects of SiO_2 on nanofibers achieved by one-step electrospinning versus the electrospinning-electrospray synergistic process, SEM images and EDS energy spectrum analysis results are shown in Fig. 4.

As shown in Fig. 4a, SiO_2 particles on the SPD-I film are predominantly encapsulated within the fiber filaments, thereby hindering effective modification of the fiber surfaces. In contrast, SiO_2 particles are distinctly distributed on the SPD-II fibers, as illustrated in Fig. 4b Through in-situ electrospray technology, SiO_2 particles from the outer channel were uniformly atomized and synchronously deposited onto the surface of the inner core-spinning fiber (PCL/DCOIT), forming a protrusive particle structure. Their hydrophobic characteristics effectively modify the fiber surface. Simultaneously, in situ atomized deposition prevented pore blockage caused by excessive coating thickness, facilitating the penetration and injection of subsequent substances such as lubricating oil. The EDS spectrum in Fig. 4c further verifies the effective encapsulation of SiO_2 within the fibers. This confirms that the electrospinning-electrospray in situ process can firmly attach SiO_2 particles to the nanofibers, ensuring their stability and functionality in the film matrix.

As shown by the characterization results in Fig. 4 above, the SPD-II nanofiber film prepared by the in situ process demonstrates superior encapsulation efficiency and surface modification compared to the SPD-I film fabricated by the traditional one-step electrospinning. These results provide a solid foundation for further optimization and promotion of this process in practical applications.

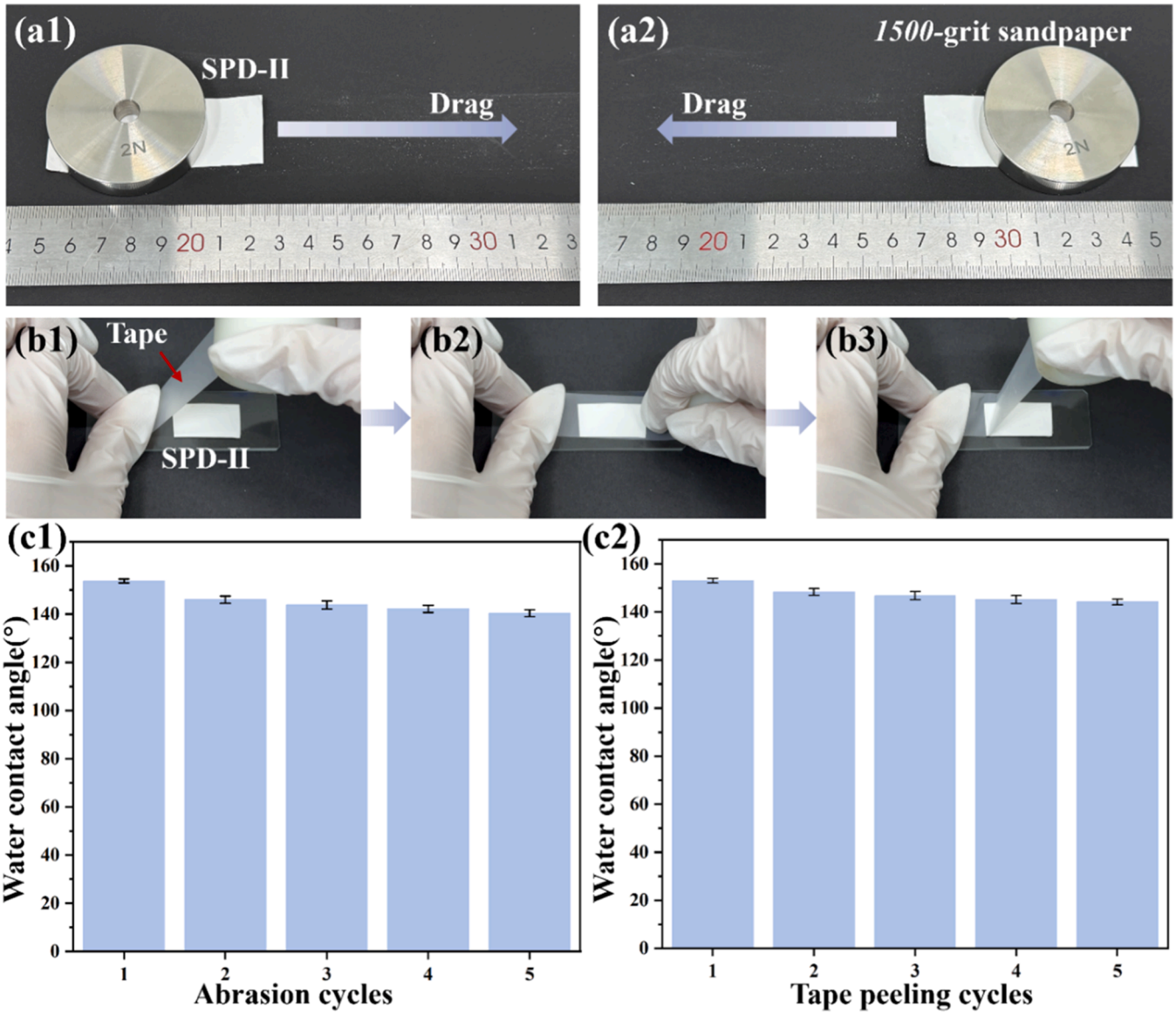

Fig. 7. (a1-a2) Sandpaper wear test of SPD-II fiber film; (b1-b3) tape stripping test; (c1-c2) contact angle after wear and peel.

3.3. *Hydrophobic and self-cleaning properties of fibrous film*

Although polymeric materials exhibit favorable mechanical properties and processability for fiber formation, their surface wettability often remains suboptimal. Surface modification has been identified as a key factor in promoting the development and practical implementation of superhydrophobic electrospun fibers [36–38]. Notably, both poly (ε-caprolactone) (PCL) and silicon dioxide (SiO_2) used in our composite system are inherently hydrophobic components, thereby endowing the resultant films with exceptional hydrophobicity. To systematically evaluate the surface hydrophobic properties, static water contact angle (WCA) measurements were quantitatively performed on three distinct nanofiber films: pristine PCL/DCOIT, SPD-I particle modified, and SPD-II particle modified films. The comparative results are summarized in Fig. 5.

As shown in Fig. 5, the water contact angle of PCL/DCOIT nanofiber films gradually decreased from 130.1° to 111.85° with increasing PCL concentration. This trend can be attributed to the rise in the spinning concentration, which results in an increase in the diameter of the PCL/DCOIT nanofiber. It is well established that a smaller fiber diameter enhances the surface roughness of the material, and a higher surface roughness is one of the critical factors for achieving superhydrophobicity [39]. This observation aligns with our choice of 15 % (w/v) PCL as the optimal concentration for subsequent film modification. Additionally, the water contact angles of SPD-I and SPD-II modified nanofiber films were measured at 133° and 153.8°, respectively. For SPD-I prepared by one-step electrospinning, the incorporation of SiO_2 moderately enhanced hydrophobicity of the film; however, most particles remained encapsulated within the electrospun fibers, limiting the efficacy of modification. In contrast, the water contact angle of SPD-II nanofiber film prepared using the in situ electrospinning-electrospray process was significantly enhanced to approximately 153.8°, demonstrating superior hydrophobic performance. These results confirm the efficacy of the in situ process technique for SiO_2 encapsulation. Furthermore, the self-cleaning performance of the SPD-II nanofiber films was evaluated, with the results presented in Fig. 6.

As observed in Figs. 6(a)-(b), water droplets rolling across the sample surface rapidly adsorbed and removed surface contaminants, leaving no detectable stains. Fig. 6(c) indicates that the film sample exhibited no blue traces after immersion in a methylene blue-stained aqueous solution. Collectively, the results presented in Figs. 6(a)-(c) demonstrate the film surface's capability to effectively prevent pollutant adhesion and

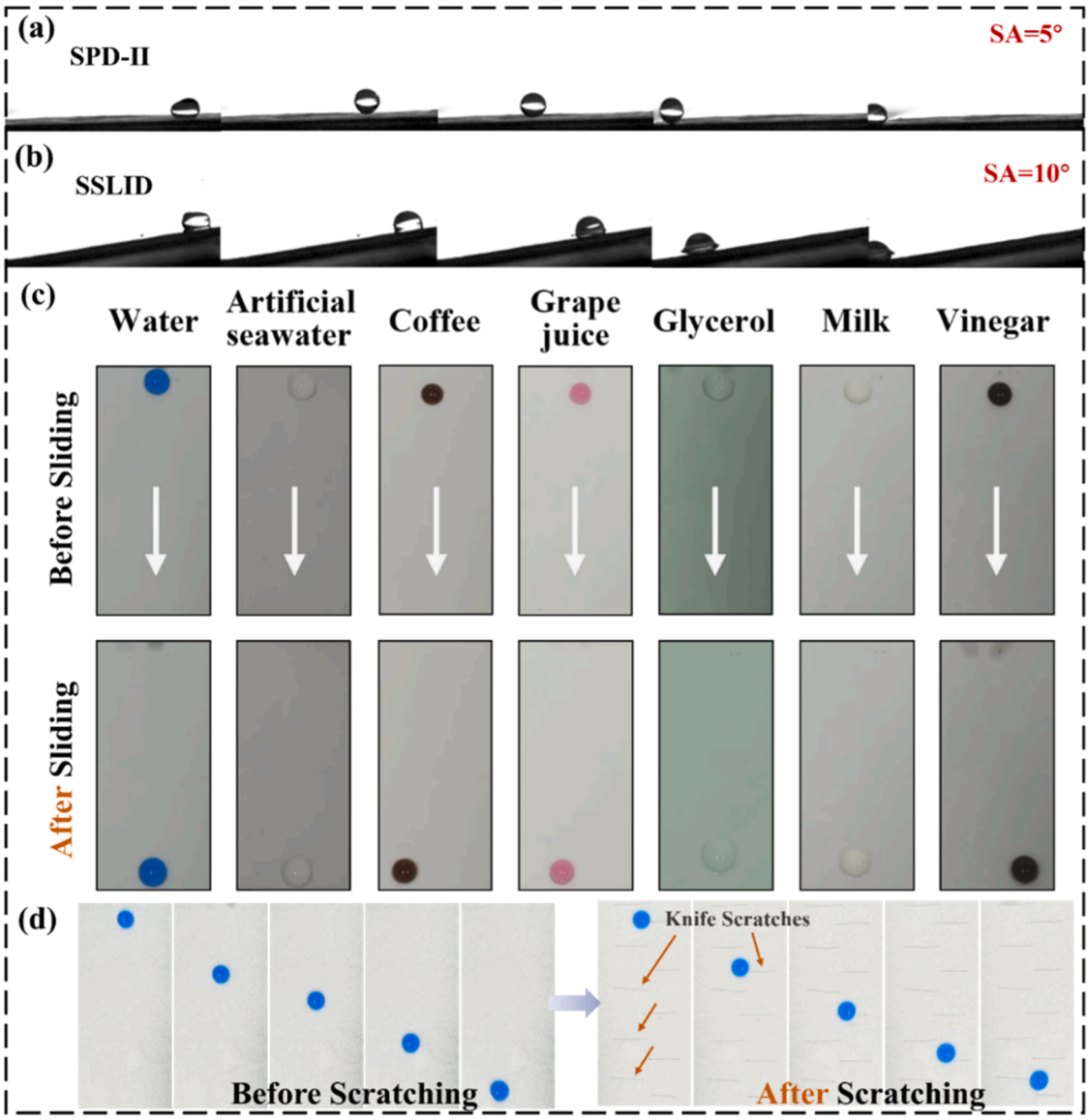

Fig. 8. The roll-off adhesion resistance of SPD-II nanofiber film (a) and SSLID composite films (b); (c) Top-view sliding behavior of multiple liquid droplets on the SSLID surface; (d) Time-lapse sequences of water droplet sliding on SSLID surfaces pre- and post-scraping (imaging interval: 0.1 s).

maintain cleanliness, thereby validating the exceptional self-cleaning properties and antifouling performance of the SPD-II nanofiber film.

3.4. *Mechanical durability of the modified fibrous film*

In practical application environments, antifouling functional layers are frequently subjected to abrasion from external contaminants such as sewage and sediment, compromising their long-term antifouling performance. Therefore, poor stability and insufficient durability remain critical bottlenecks hindering the development of superhydrophobic electrospun film technology. The electrospinning-electrospray in situ process, however, offers a potential solution to address this significant challenge.

To evaluate the mechanical stability of the SPD-II nanofiber film, samples were subjected to controlled dragging tests on 1500-grit sandpaper and standardized tape peeling experiments. Post-test water contact angle measurements were performed to assess surface property retention, with the testing procedures and results detailed in Fig. 7.

Figs. 7(a)-(b) illustrate the experimental procedures, and Fig. 7(c) displays the water contact angle variations after mechanical stress. As seen in Fig. 7(c), the water contact angles of the samples decreased by approximately 10.3 % and 7.15 % after sandpaper abrasion and tape peeling cycles, respectively. These observations demonstrate the superior wear resistance of the SPD-II coating. Even when external nanoparticles on the fiber surface were abraded, the exposed internal fibers retained encapsulated SiO_2 particle structures, thereby ensuring sustained hydrophobicity under mechanical degradation.

3.5. *Anti-adhesion and stability of super-slippery drug-loaded modified film*

The modified SPD-II nanofiber films demonstrated remarkable superhydrophobic properties and mechanical stability. Subsequently, SSLID composite films with enhanced antifouling strategies were fabricated through the infusion of lubricating oil. A systematic evaluation of their anti-adhesion and stability was conducted, as illustrated in Fig. 8.

As shown in Fig. 8a, water droplets rapidly roll off the SPD-II film surface at a sliding angle of 5°, demonstrating ultralow surface adhesion. This indicates that a uniform and stable hydrophobic structure is formed on the surface of the SPD-II film, which effectively prevents water

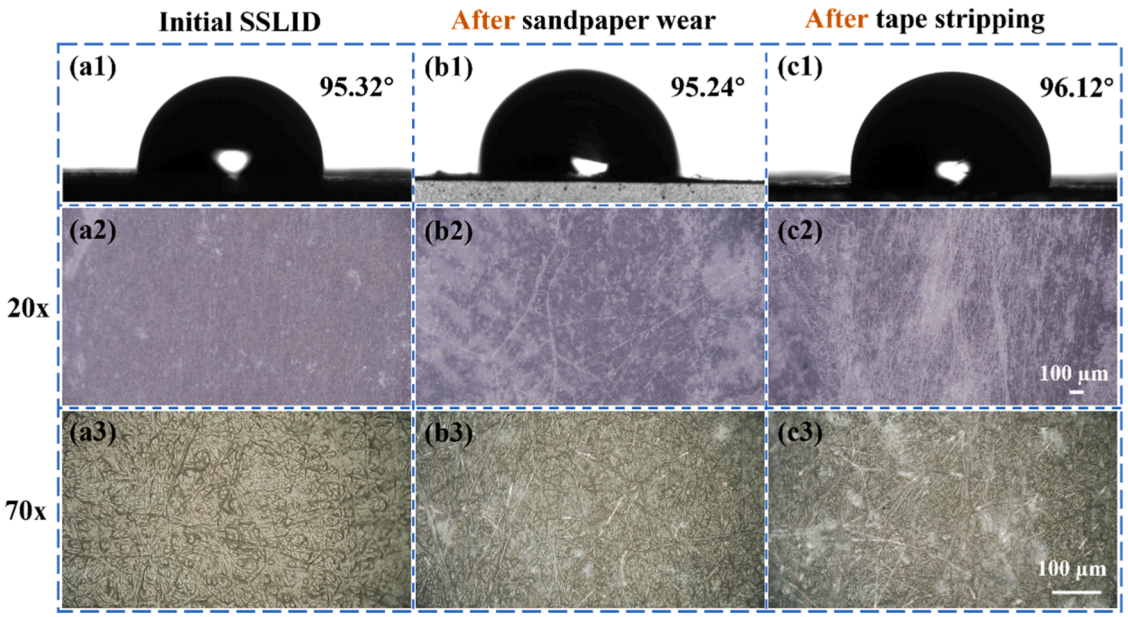

Fig. 9. Water contact angles of samples in different states and surface morphology images at macroscopic (20x) and microscopic (70x) levels: (a1-a3) Initial SSLID; (b1-b3) SSLID after five times of sandpaper wear; and (c1-c3) SSLID after five times of tape stripping.

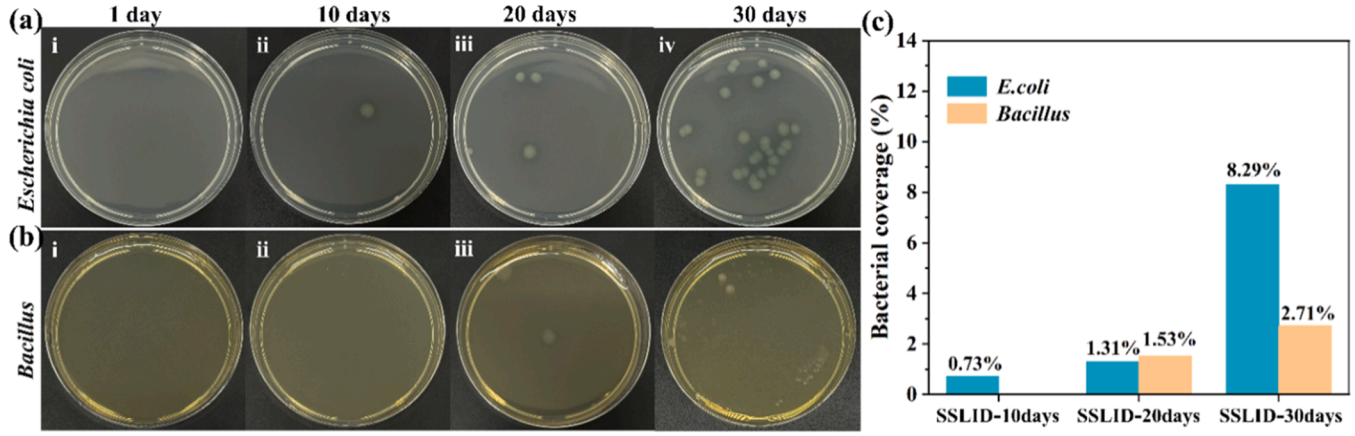

Fig. 10. Agar plate images of (a)*E. coli* and (b) *Bacillus* (i-iv: immersion durations of 1,10,20, and 30 days, respectively); (c) Statistical histogram of the coverage of the two types of bacteria.

droplets from remaining on the film surface. Following lubricant infusion into the SPD-II film, droplets slide effortlessly from the SLIPS surface at a tilt angle of 10° (Fig. 8b). These observations confirm that the lubricant infiltrates the micro-nano porous structures through capillary action, forming a continuous lubricating layer that enables smooth droplet sliding on the oil-impregnated surface. Meanwhile, the FTIR spectra also clearly show the reasons for the superhydrophobicity of the SPD-II and SSLID samples. The methyl functional groups of the modified particles and lubricating oil play an important role (see supplementary file Figure S1). Fig. 8(c) demonstrates the sliding performance of various fluids (seawater, coffee, grape juice, glycerol, milk, vinegar) on the SSLID surface. Through the top-down view, these droplets are observed to slide smoothly off the 10°-tilted SSLID composite surface within seconds, further validating its ultralow adhesion properties. Additionally, no lubricant layer delamination or failure occurred even after repeated exposure to multiple liquids, indicating that the oil film and micro/nano porous structure on the surface of SSLID remain stable.

Considering the possible extreme working conditions, the antifouling coating may be subject to damage such as tearing and splitting. The stability of this damage was evaluated through blade scratching tests, and sequential images of water droplet sliding before and after scratches on the SSLID surface were documented, with the results presented in Fig. 8d It is evident from the figure that the scraping blade induces physical damage to the slippery surface, but waterdrops still easily slipped off the inclined surface. This shows that the SSLID coating effectively maintains its superhydrophobicity and exhibits exceptional damage resistance.

Meanwhile, this study measured the changes in water contact angle of the SSLID samples before and after sandpaper wear and tape stripping, and characterized changes in morphology to analyze the lubrication stability of SSLID after oil injection. Since the SSLID samples were in an oil-absorbed state, oil molecules would be squeezed out and evaporate under vacuum, making it impossible to capture the morphology using SEM. We chose a high-resolution digital microscope (HRX-01, Hirox, Japan) to capture morphology images. The test operation was consistent with that of the SPD-II sample, and the contact angle and image results are shown in Fig. 9.

From the contact angle results in the first row of Fig. 9, it can be seen that the contact angles before and after wear remain at approximately 95°, which is precisely the contact angle of lubricating oil. This result

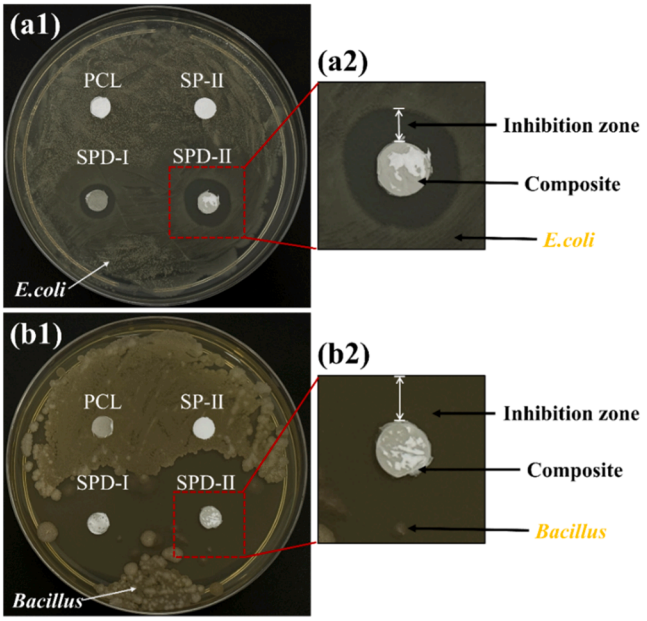

Fig. 11. Antibacterial inhibition analysis: (a1) Comparative inhibition zones of various samples against *E. coli*; (a2) Enlarged image of the SPD-II film against *E. coli*; (b1) Comparative inhibition zones of various samples against *Bacillus*; (b2) Enlarged image of the SPD-II film against *Bacillus*.

demonstrates that lubricating oil can be rapidly replenished in porous structures through capillary action, thereby maintaining anti-adhesion properties. From the macroscopic optical image in the second row, it can be seen that the surface has some delamination and scratches. However, from the microscopic image in the third row, it is observed that the blending state of the lubricating oil and the fibers remains largely unchanged, and the lubricating oil still wets the fiber pores. This further explains the reason why the contact angle before and after wear can basically remain in a hydrophobic state. In addition, the flow shear experimental data also showed the low adhesion stability of the lubrication layer on the surface of SSLID films (see supplementary file Figure S2). The remarkable stability primarily stems from the self-healing mechanism of the lubricant layer. Upon surface damage, capillary-driven flow enables rapid lubricant redistribution within the nanoporous structure, autonomously replenishing compromised regions to restore surface integrity and functionality [40,41]. This distinctive self-repair capability ensures prolonged retention of ultralow adhesion and antifouling performance, endowing the SSLID film with outstanding durability and practical value even under harsh marine environments.

3.6. Antifouling test

The antifouling performance of the modified composite films was evaluated using two bacterial strains [42]: *E. coli* and *Bacillus* sp., with experimental results shown in Figs. 10-12, respectively.

3.6.1. Anti-adhesion test

The antifouling performance of SSLID modified composite films at 37 °C was evaluated through immersion testing. SSLID samples were immersed in bacterial suspensions containing *E. coli* and *Bacillus* for 1, 10, 20, and 30 days to systematically investigate their antibacterial adhesion resistance. Bacterial colony counts on agar plates were determined via the plate counting method, while surface coverage rates were quantitatively analyzed using ImageJ image analysis software. The experimental results are presented in Fig. 10.

As shown in Figs. 10 (a-b), bacterial colony counts on agar plates demonstrated a gradual increase with extended immersion time, a trend further substantiated by the histogram statistics in Fig. 10c. Specifically, no *E. coli* or *Bacillus* colonies were detected on agar plates for samples immersed for 1 day, which indicates the excellent short-term antifouling efficacy of SSLID. When the soaking duration was extended, the number of colonies increased slightly, with the coverage rates reaching 1.31 % (*E. coli*) and 1.53 % (*Bacillus*) at 20 days, respectively. By 30 days, the coverage rates had risen to 8.29 % and 2.71 %, respectively, showing stable antifouling performance over time. Further analysis revealed that the long-term antifouling capability of the SSLID films is primarily attributed to their distinctive surface structure and chemical properties. The lubricant-infused slippery surface minimizes bacterial contact area, effectively inhibiting adhesion [43], while sustained drug release from the loaded film ensures continuous antifouling functionality. The synergistic interplay of these attributes enables the SSLID modified

Table 2
Statistics of inhibition zone size of different nanofiber samples against *E. coli* and *Bacillus*.

Strain	Zones of Inhibition (mm)			
	PCL	SP-II	SPD-I	SPD-II
E.coli	0	0	1.63±0.17	3.49±0.42
Bacillus	0	0	11.77±1.99	14.51±1.9

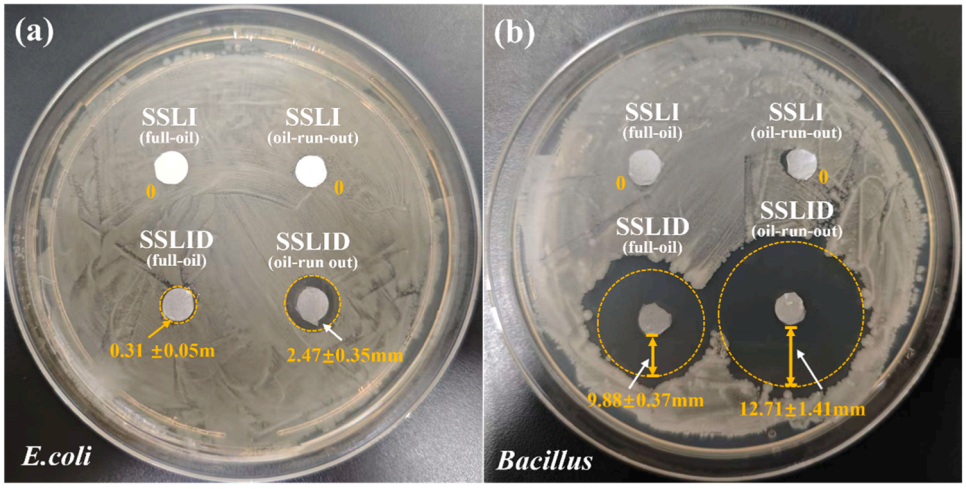

Fig. 12. Antibacterial inhibition statistics and analysis: (a) Comparative inhibition zones of various samples against *E. coli*; (b) Comparative inhibition zones of various samples against *Bacillus*.

composite films to retain superior antifouling performance under prolonged immersion.

Notably, *Bacillus* adhesion remained consistently lower than that of *E. coli* throughout the experiment, likely attributable to differences in bacterial surface characteristics. Although the ultralow adhesion surface of the SSLID composite film effectively suppresses initial bacterial attachment, species-specific responses were observed. The hydrophobic surface of *Bacillus* may hinder stable adhesion on the SSLID surface, whereas *E. coli*—with its hydrophilic surface and fimbriae structure—exhibits a greater propensity for initial surface colonization.

3.6.2. Antibacterial test of nanofiber matrix and oil-injected film

To investigate the antibacterial performance of modified composite films after complete depletion of the surface lubricant layer, additional antimicrobial tests were performed on both drug-loaded and drug-free nanofiber matrix and oil-injected films. In the experiment, *E. coli* and *Bacillus* strains were employed to assess the antibacterial efficacy of the fibrous film. After incubation at 37 °C for 24 h, the formation of an inhibition zone was observed, and its diameter served as a direct indicator of the antibacterial activity strength of the sample. The experimental results are shown in Fig. 11 and Fig. 12.

As shown in Fig. 11, all SPD-I/II containing DCOIT formed distinct inhibition zones on the surface of the medium, demonstrating significant antibacterial properties. As a highly effective antibacterial agent, DCOIT can be continuously released from the fibrous film and effectively inhibits the growth and reproduction of bacterial colonies. In contrast, no obvious inhibition zones were observed around the two drug-free control groups: PCL and SP-II nanofiber films without DCOIT, indicating that they did not play an effective role in inhibiting bacterial growth. Quantitative results of the inhibition zones are summarized in Table 2.

From the data presented in Table 2, it is evident that neither PCL nor SP-II nanofiber films exhibited any antibacterial activity. This suggests that although nanofiber films possess a certain degree of hydrophobicity, they are unable to exert effective antibacterial effects in the absence of DCOIT. In contrast, SPD-I and SPD-II nanofiber films containing DCOIT demonstrated significant antibacterial activity, which is closely related to their specific antibacterial mechanisms. In fact, antibacterial performance generally depends on active agents such as DCOIT, whose unique chemical structure enables efficient binding to bacterial cell walls, followed by cellular internalization and subsequent interactions with sulfur-containing proteins. These interactions disrupt normal cellular physiological functions, thereby suppressing bacterial growth [44]. In this study, the SPD-II nanofiber films exhibited inhibition zones of 3.49 ± 0.42 mm against *E. coli* and 14.51 ± 1.9 mm against *Bacillus*, significantly larger than those of the SPD-I samples (1.63 ± 0.17 mm and 11.77 ± 1.99 mm, respectively). This corresponds to antibacterial efficacy improvements of approximately 113.5 % (*E. coli*) and 23.3 % (*Bacillus*). The observed differences in efficacy indicate that the distribution pattern of DCOIT plays a crucial role in determining its antibacterial performance. The SPD-II film was fabricated using the electrospinning-electrospray in situ process, ensuring uniform DCOIT distribution on fiber surfaces while preventing encapsulation within fibers or particles. This structural configuration allows DCOIT to efficiently interact with bacterial cells, maximizing its antibacterial efficacy. Consequently, the SPD-II modified film demonstrates superior performance in suppressing bacterial growth compared to other samples. These results further validate the importance of fabrication methodologies in determining antibacterial outcomes and provide valuable insights for optimizing the design and application of antifouling films.

Antibacterial inhibition result of the oil-injected samples SSLID under both full-oil and oil-run-out conditions is shown in Fig. 12. The oil-injected fiber films SSLI without any drug as the control group.

As can be seen from Fig. 12, the drug-free samples show no antibacterial effect at all which is consistent with the antibacterial effect of the drug-free nanofibrous. However, the antibacterial results of the SSLID samples in the full-oil state and the oil-run-out state exceeded our expectations. The antibacterial zones indicate that the SSLID samples had a certain antibacterial effect on *E. coli* even when fully filled with oil, and the effect is even stronger on *Bacillus*. The specific size of the antibacterial zone is indicated by the values in the Figure. We assess that although silicone oil slowed down the drug elution rate, the drug was not actively released into the culture medium. Dimethyl silicone oil might have adsorbed or encapsulated the drug on the surface of the matrix during the preparation stage, resulting in the formation of a local high concentration area of the drug on the surface within the 24-hour test period. When bacteria approached, trace amounts of drugs might have exerted antibacterial effects through diffusion or contact transmission. Moreover, when the lubricating oil ran out, the antibacterial drugs fully exert their effects and could also form an antibacterial zone

In summary, the DCOIT-loaded SPD-II nanofiber film demonstrates remarkable efficacy in suppressing bacterial colonization and growth. This antimicrobial performance stems not only from the inherent chemical activity of DCOIT but also benefits from the exceptionally high specific surface area of the nanofiber film, which provides abundant interaction sites for enhanced antibacterial effectiveness. Based on the anti-fouling test results of SSLID samples in their two states, it is evident that the dual-mechanism strategy—reducing bacterial adhesion and colonization in the initial stage, followed by sustained inhibition of bacterial proliferation—exhibits a synergistic antibacterial effect, particularly through early-stage drug action. These findings further validate the effectiveness of the "multi-mechanism synergistic antifouling" strategy proposed in this study.

4.Conclusion

In this study, an electrospinning-electrospray in-situ synergy process was adopted to successfully fabricate an anti-adhesive drug-loaded antifouling film. The resulting three-dimensional micro/nano porous network structure within the film matrix not only serves as a stable reservoir for lubricants but also effectively inhibits the initial settlement and adhesion of bacteria with its ultra-low surface adhesion and superlubricity. Upon depletion of the lubricant, the drug-loaded fiber matrix releases the antifouling agent DCOIT through sustained release dynamically, achieving long-term antifouling. The synergy antifouling film under dual mechanisms also has a unique self-adaptive reconstruction ability due to capillary action, maintaining surface lubrication even in case of damage and consumption. This process strategy provides an innovative solution for the development of environmentally friendly antifouling films and has significant application potential in fields such as ship antifouling and medical devices.

CRediT authorship contribution statement

Fengqin Li: Writing – review & editing, Writing – original draft, Supervision, Resources. **Yang Zhou:** Validation, Investigation, Data curation. **Yuxue Hu:** Methodology, Formal analysis. **Xiaoming Feng:** Resources, Project administration. **Guizhong Tian:** Supervision, Project administration, Formal analysis.

Declaration of competing interest

The authors declare that they have no known competing financial interests or personal relationships that could have appeared to influence the work reported in this paper.

Acknowledgments

This work was supported by the National Natural Science Foundation of China (No. 52305605 and 52375291) and the Natural Science Foundation of the Jiangsu Higher Education Institutions of China (No. 22KJB430022).

Supplementary materials

Supplementary material associated with this article can be found, in the online version, at doi:10.1016/j.surfin.2025.107196.

Data availability

Data will be made available on request.

References

[1] X. Wang, J. Yang, X. Jiang, L. Yu, Preparation and properties of environmentally friendly marine antifouling coatings based on a collaborative strategy, Langmuir. 38 (2022) 6676–6689, https://doi.org/10.1021/acs.langmuir.2c00612.

[2] J. Yuan, Q. Gu, G. Zheng, J. Yang, W. Zhao, Y. Wu, Novel environment-friendly grease-infused porous surface exhibiting long-term cycle effective antifouling performance, Colloids Surf. A: Physicochem. Eng. Asp. 627 (2021) 127196, https://doi.org/10.1016/j.colsurfa.2021.127196.

[3] J. Pan, Q. Xie, H. Chiang, Q. Peng, P.-Y. Qian, C. Ma, G. Zhang, From the nature for the nature": an eco-friendly antifouling coating consisting of poly(lactic acid)-based polyurethane and natural antifoulant, ACS. Sustain. Chem. Eng. 8 (2019) 1671–1678, https://doi.org/10.1021/acssuschemeng.9b06917.

[4] X. Liu, J.L. Yang, D. Rittschof, J.S. Maki, J.D. Gu, Redirecting marine antibiofouling innovations from sustainable horizons, Trends. Ecol. Evol. 37 (2022) 469–472, https://doi.org/10.1016/j.tree.2022.02.009.

[5] Rosaria Ciriminna, Frank V. Bright, M. Pagliaro, Ecofriendly antifouling marine coatings, ACS. Sustain. Chem. Eng. 3 (2015) 559–565, https://doi.org/10.1021/sc500845n.

[6] Q. Li, Q. Yang, Z. Cao, X. Le, F. Meng, Y. Ren, Q. Liu, Q. Zhang, Enhanced antifouling performance with a synergistic effect of self-renewal antifouling and contact bacteriostasis via the ionic exchange, Prog. Org. Coat. 192 (2024) 108471, https://doi.org/10.1016/j.porgcoat.2024.108471.

[7] Y.-Y. Quan, Z. Chen, Y. Lai, Z.-S. Huang, H. Li, Recent advances in fabricating durable superhydrophobic surfaces: a review in the aspects of structures and materials, Mater. Chem. Front. 5 (2021) 1655–1682, https://doi.org/10.1039/d0qm00485e.

[8] H. Jin, L. Tian, W. Bing, J. Zhao, L. Ren, Bioinspired marine antifouling coatings: status, prospects, and future, Prog. Mater. Sci. 124 (2022) 100889, https://doi.org/10.1016/j.pmatsci.2021.100889.

[9] Z. Li, P. Liu, S. Chen, X. Liu, Y. Yu, T. Li, Y. Wan, N. Tang, Y. Liu, Y. Gu, Bioinspired marine antifouling coatings: antifouling mechanisms, design strategies and application feasibility studies, Eur. Polym. J. 190 (2023) 111997, https://doi.org/10.1016/j.eurpolymj.2023.111997.

[10] Z. Tong, Q. Rao, S. Chen, L. Song, J. Hu, Y. Hou, X. Gao, J. Lu, X. Zhan, Q. Zhang, Sea slug inspired smart marine antifouling coating with reversible chemical bonds: controllable UV-responsive coumarin releasing and efficient UV-healing properties, Chem. Eng. J. 429 (2022) 132471, https://doi.org/10.1016/j.cej.2021.132471.

[11] L. Zhao, R. Chen, J. Liu, Q. Liu, J. Yu, J. Zhu, P. Liu, J. Wang, Layer-by-layer-assembled biomimetic microstructure surface with multiple synergistic antifouling performance, Prog. Org. Coat. 183 (2023) 107812, https://doi.org/10.1016/j.porgcoat.2023.107812.

[12] J. Li, H. Lin, J. Li, Y. Wang, Engineered lubricative lecithin-based electrospun nanofibers for the prevention of postoperative abdominal adhesion, Pharmaceutics. 16 (2024) 1562, https://doi.org/10.3390/pharmaceutics16121562.

[13] J. Wang, C. You, Y. Xu, T. Xie, Y. Wang, Research advances in electrospun nanofiber membranes for non-invasive medical applications, Micromachines. (Basel) 15 (2024) 1226, https://doi.org/10.3390/mi15101226.

[14] Weili Shao, Simeng Liu, Kai Wang, Jingyi Niu, Liang Zhu, Shengli Zhu, Gaihuan Ren, Xu Wang, Ying Cao, Hui Zhang;, et al., Using modified raw materials to fabricate electrospun, superhydrophobic poly(lactic acid) multiscale nanofibrous membranes for air-filtration applications, Sep. Purif. Technol. (2024), https://doi.org/10.1016/j.seppur.2023.125872.

[15] D. Li, Z. Lin, J. Zhu, J. Yu, J. Liu, Z. Liu, R. Chen, Q. Liu, P. Liu, J. Wang, An engineering-oriented approach to construct rough micro/nano-structures for anticorrosion and antifouling application, Colloids Surf. A: Physicochem. Eng. Asp. 621 (2021) 126590, https://doi.org/10.1016/j.colsurfa.2021.126590.

[16] Y. Kong, W. Zhang, T. He, X. Yang, W. Bi, J. Li, W. Yang, W. Chen, Asymmetric wettable polycaprolactone-chitosan/chitosan oligosaccharide nanofibrous membrane as antibacterial dressings, Carbohydr. Polym. 304 (2023) 120485, https://doi.org/10.1016/j.carbpol.2022.120485.

[17] D. Ji, Y. Lin, X. Guo, B. Ramasubramanian, R. Wang, N. Radacsi, R. Jose, X. Qin, S. Ramakrishna, Electrospinning of nanofibres, Nat. Rev. Methods Primers (2024) 4, https://doi.org/10.1038/s43586-023-00278-z.

[18] X. Lan, H. Wang, J. Bai, X. Miao, Q. Lin, J. Zheng, S. Ding, X. Li, Y. Tang, Multidrug-loaded electrospun micro/nanofibrous membranes: fabrication strategies, release behaviors and applications in regenerative medicine, J. Control Release 330 (2021) 1264–1287, https://doi.org/10.1016/j.jconrel.2020.11.036.

[19] J. Xing, M. Zhang, X. Liu, C. Wang, N. Xu, D. Xing, Multi-material electrospinning: from methods to biomedical applications, Mater. Today Bio. 21 (2023) 100710, https://doi.org/10.1016/j.mtbio.2023.100710.

[20] L. Jianxin, C. Xuedi, Z. Xiaolei, J. Xicheng, Y. Hengzhe, F. Junlin, Review on functional electrospun nanofibers: theory, application and fabrication, Mater. Sci. Eng.: B 307 (2024) 117488, https://doi.org/10.1016/j.mseb.2024.117488.

[21] B.N. Blackstone, J.J. Willard, C.H. Lee, M.T. Nelson, R.T. Hart, J.J. Lannutti, H. M. Powell, Plasma surface modification of electrospun fibers for adhesion-based cancer cell sorting, Integr. Biol. 4 (2012) 1112, https://doi.org/10.1039/c2ib20025b.

[22] Y. Xue, Z. Zheng, S. Shen, G. Liu, R.X. Xu, Combinatory electrospray and electrospinning to produce multi-layered membrane with enhanced mechanical property, Environ. Eng. Res. 28 (2022), https://doi.org/10.4491/eer.2022.023, 220023-220020.

[23] Y. Si, S. Shi, J. Hu, Electrospinning and electrospraying synergism: twins-tech collaboration across dimensions, Matter. 7 (2024) 1373–1405, https://doi.org/10.1016/j.matt.2024.01.009.

[24] A. Borchers, T. Pieler, Programming pluripotent precursor cells derived from Xenopus embryos to generate specific tissues and organs, Genes. (Basel) 1 (2010) 413–426, https://doi.org/10.3390/genes1030413.

[25] Y. Si, J. Yang, D. Wang, S. Shi, C. Zhi, K. Huang, J. Hu, Bioinspired hierarchical multi-protective membrane for extreme environments via Co-electrospinning-electrospray strategy, Small. (2023) 20, https://doi.org/10.1002/smll.202304705.

[26] Y. Wang, J. Xu, Y. Shen, C.-a. Wang, Z. Zhang, F. Li, J. Cheng, Y. Ye, R. Shen, Fabrication of energetic aluminum core/hydrophobic shell nanofibers via coaxial electrospinning, Chem. Eng. J. 427 (2022) 132001, https://doi.org/10.1016/j.cej.2021.132001.

[27] J. Gao, K. Zhang, H. Li, C. Lang, L. Zhang, Eco-friendly intrinsic self-healing superhydrophobic polyurea/TiO2 composite coatings for underwater drag reduction and antifouling, Prog. Org. Coat. 183 (2023) 107769, https://doi.org/10.1016/j.porgcoat.2023.107769.

[28] S. Pourhashem, A. Seif, F. Saba, E.G. Nezhad, X. Ji, Z. Zhou, X. Zhai, M. Mirzaee, J. Duan, A. Rashidi, et al., Antifouling nanocomposite polymer coatings for marine applications: a review on experiments, mechanisms, and theoretical studies, J. Mater. Sci. Technol. 118 (2022) 73–113, https://doi.org/10.1016/j.jmst.2021.11.061.

[29] H. Zhang, F. Wang, Z. Guo, The antifouling mechanism and application of bio-inspired superwetting surfaces with effective antifouling performance, Adv. Colloid. Interface Sci. 325 (2024) 103097, https://doi.org/10.1016/j.cis.2024.103097.

[30] X. Liu, L. Chen, Q. Dong, Z. Wang, D. Zhang, J. He, Y. Ye, J. Zhou, W. Zhu, Z. Hu, et al., Emerging starch composite nanofibrous films for food packaging: facile construction, hydrophobic property, and antibacterial activity enhancement, Int. J. Biol. Macromol. 222 (2022) 868–879, https://doi.org/10.1016/j.ijbiomac.2022.09.187.

[31] R. Ruhal, R. Kataria, Biofilm patterns in gram-positive and gram-negative bacteria, Microbiol. Res. 251 (2021) 126829, https://doi.org/10.1016/j.micres.2021.126829.

[32] X. Yuan, Y. Wang, L. Liu, H. Dong, G. Yang, Hydrophilic tyrosine-based phenolic resin with micro-ripples morphology for marine antifouling application, Colloids. Surf. B Biointerfaces. 217 (2022) 112672, https://doi.org/10.1016/j.colsurfb.2022.112672.

[33] R.K. Mishra, P. Mishra, K. Verma, A. Mondal, R.G. Chaudhary, M.M. Abolhasani, S. Loganathan, Electrospinning production of nanofibrous membranes, Env. Chem Lett 17 (2018) 767–800, https://doi.org/10.1007/s10311-018-00838-w.

[34] S. Higashi, T. Hirai, M. Matsubara, H. Yoshida, A. Beniya, Dynamic viscosity recovery of electrospinning solution for stabilizing elongated ultrafine polymer nanofiber by TEMPO-CNF, Sci. Rep. 10 (2020) 13427, https://doi.org/10.1038/s41598-020-69136-2.

[35] C. Fan, Z. Long, Y. Zhang, A. Mensah, H. He, Q. Wei, P. Lv, Robust integration of energy harvesting with daytime radiative cooling enables wearing thermal comfort self-powered electronic devices, Nano Energy 116 (2023) 108842, https://doi.org/10.1016/j.nanoen.2023.108842.

[36] N. Nuraje, W.S. Khan, Y. Lei, M. Ceylan, R. Asmatulu, Superhydrophobic electrospun nanofibers, J. Mater. Chem. A 1 (2013) 1929–1946, https://doi.org/10.1039/c2ta00189f.

[37] S. Subhash Latthe, A. Basavraj Gurav, C. Shridhar Maruti, R. Shrikant Vhatkar, Recent progress in preparation of superhydrophobic surfaces: a review, J. Surf. Eng. Mater. Adv. Technol. 02 (2012) 76–94, https://doi.org/10.4236/jsemat.2012.22014.

[38] R.S. Kurusu, N.R. Demarquette, Surface modification to control the water wettability of electrospun mats, Int. Mater. Rev. 64 (2018) 249–287, https://doi.org/10.1080/09506608.2018.1484577.

[39] G. Zhang, P. Wang, X. Zhang, C. Xiang, L. Li, The preparation of PCL/MSO/SiO2 hierarchical superhydrophobic mats for oil-water separation by one-step method, Eur. Polym. J. 116 (2019) 386–393, https://doi.org/10.1016/j.eurpolymj.2019.04.011.

[40] C. Liu, Y. Li, C. Lu, Y. Liu, S. Feng, Y. Liu, Robust slippery liquid-infused porous network surfaces for enhanced anti-icing/deicing performance, ACS. Appl. Mater. Interfaces. 12 (2020) 25471–25477, https://doi.org/10.1021/acsami.0c05954.

[41] F. Chen, Y. Wang, Y. Tian, D. Zhang, J. Song, C.R. Crick, C.J. Carmalt, I.P. Parkin, Y. Lu, Robust and durable liquid-repellent surfaces, Chem. Soc. Rev. 51 (2022) 8476–8583, https://doi.org/10.1039/d0cs01033b.

[42] I. Banerjee, R.C. Pangule, R.S. Kane, Antifouling coatings: recent developments in the design of surfaces that prevent fouling by proteins, bacteria, and marine

organisms, Adv. Mater. 23 (2011) 690–718, https://doi.org/10.1002/adma.201001215.
[43] F. Li, Y. Hu, X. feng, G. Tian, Environmentally friendly SLIPS coating based on flexible sponge: a novel approach to antifouling for ships, Colloids Surf. A: Physicochem. Eng. Asp. 695 (2024) 134218, https://doi.org/10.1016/j.colsurfa.2024.134218.
[44] A.M. El-Shamy, T.Y. Soror, H.A. El-Dahan, E.A. Ghazy, A.F. Eweas, Microbial corrosion inhibition of mild steel in salty water environment, Mater. Chem. Phys. 114 (2009) 156–159, https://doi.org/10.1016/j.matchemphys.2008.09.003.